Chapter Three

Review of Optical Fibre Sensing

Over the last few decades, the field of optics has been applied to high speed communication systems with the use of optical fibres to transmit encoded optical signals. In this chapter a spin-off from this technology, namely, the application of optical fibres to measurement, is reviewed. Section 3.1 gives an overview of optical fibre (OF) sensors and their uses in many fields. An important sub-section of OF sensing concerns those sensors based on interferometry and Section 3.1.1 reviews the principles of optical fibre interferometry. Of particular relevance to the measurement of corona wind speed is the use of OF sensing for temperature and velocity measurement and these are described in Sections 3.2 and 3.3, respectively.

Hot-wire anemometers have long been used to measure the speed of fluid flows and have been employed in the measurement of the speed of the corona wind (Thanh, 1979; Davidson and Shaugnessy, 1986; and Chen and Barthakur, 1991). A 'hot-fibre' anemometer, which uses a heated fibre instead of a heated wire, has been developed and is the basis of the optical fibre Fabry-Perot sensor which is used in this study of the corona wind. This 'hot-fibre' anemometer is discussed in Section 3.4.

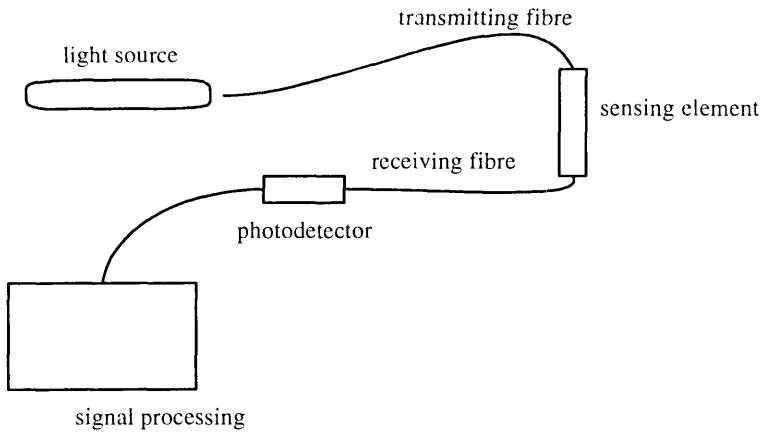

Figure 3.1 Schematic diagram of an optical fibre sensor.

3.1 Principles of optical fibre sensors

The basic concept of an OF sensor is shown in Figure 3.1. An OF sensor consists of a light source, typically a laser or LED, coupled to an optical fibre which transmits the light to a sensing element. In the sensing element light is encoded and transmitted via an optical fibre to an optical detector, typically a photodiode. The sensing element is specifically designed for the measurand of interest and may be the fibre itself or another medium.

OF sensors are grouped according to the sensing element and usually fall into one of three main groups; extrinsic, intrinsic and evanescent-field sensors. Extrinsic OF sensors make use of an optical fibre to transmit light to and from the sensing element. Examples of the sensing element of an extrinsic OF sensor are; the bulk optical component of a current sensor (Rogers, 1989; Fisher *et al.*, 1997), the chemical compound such as phenol-red dye used for blood pH monitoring (Mignani and Baldini, 1996) and the Fabry-Perot cavity used in many commercial pressure sensors (Wolthuis *et al.*, 1991).

In an intrinsic OF sensor, the sensor is constructed in such a way that the fibre itself is sensitive to one or more parameters of interest. The natural sensitivity of silica optical fibres to pressure and temperature is often exploited in the manufacture of an OF sensor, although special fibres can be

produced with enhanced, or depressed, sensitivity to specific measurands. Examples of intrinsic OF sensors are; the optical fibre gyroscope which detects rotation with respect to inertial space due to an enhanced Sagnac effect in a multi-turn single-mode fibre (Jeunhomme, 1990), acoustic sensors which use the pressure sensitivity of optical fibres to measure the magnitude and direction of an acoustic wave (Jackson, 1985) and electric field sensors produced by coating a single-mode optical fibre with a piezoelectric polymer (DeSouza and Mermelstein, 1982; Imai *et al.*, 1992).

A third group of OF sensors is the evanescent-field sensor. An optical fibre acts as a guide for the propagating wave. However, a small amount of the energy of the wave propagates outside the fibre core. The part of the wave outside the core has a finite amplitude which decays exponentially into the lower refractive index material of the cladding. This so-called evanescent field can be accessed by stripping a length of fibre of its cladding and will interact with the medium surrounding the fibre. Evanescent-field sensors can detect either the absorption of the evanescent field (Simhony *et al.*, 1986; Paul and Kychakoff, 1987) or luminescence effects in a surrounding medium (MacCraith *et al.*, 1993; Mignani and Baldini, 1996).

Each of the above groups of OF sensors can be further sub-divided depending on which property of the guided light is modulated. Thus, OF sensors are available which detect modulation by the parameter of interest of the phase, intensity, wavelength, polarisation state or spectral distribution of the transmitted light.

3.1.1 Optical fibre interferometers

Intrinsic sensors are very often used in an interferometer arrangement which is similar in configuration to that of a bulk-optics interferometer. Unlike a bulk-optics interferometer, however, an optical-fibre interferometer does not require the light to travel in straight paths as the fibre can be coiled, go round bends and can extend over a considerable distance without being subject to the alignment and stability problems that affect bulk-optic interferometers.

Each of the common unbound-beam interferometers has its optical fibre equivalent. Michelson, Mach-Zehnder, Fabry-Perot and Fizeau interferometers can all be assembled using optical fibre components. Figure 3.2 shows a schematic diagram of three commonly used optical fibre interferometers. The important component in all three arrangements is the 2 x 2 bidirectional

coupler. The Mach-Zehnder optical fibre interferometer, diagram A in Figure 3.2, is made from two of these couplers. Laser light is coupled into one arm of the first coupler and the coupler splits the light into two equal-intensity beams, one of which is transmitted through the reference fibre and the other through the sensing fibre which is subject to the measurand. The two beams are then recombined in the second coupler and the output of the interferometer can be observed at either or both of the fibre arms. An optical fibre Michelson interferometer, diagram B in Figure 3.2, requires only one coupler. One of the output arms of the coupler acts as the sensing arm and the other output arm is the reference arm of the interferometer. The Michelson optical fibre interferometer can rely on the Fresnel reflections at the cleaved ends of the two fibre arms, generated by the refractive index mismatch between silica and air, or the ends of the two fibre arms can be metal coated to provide 100% reflections.

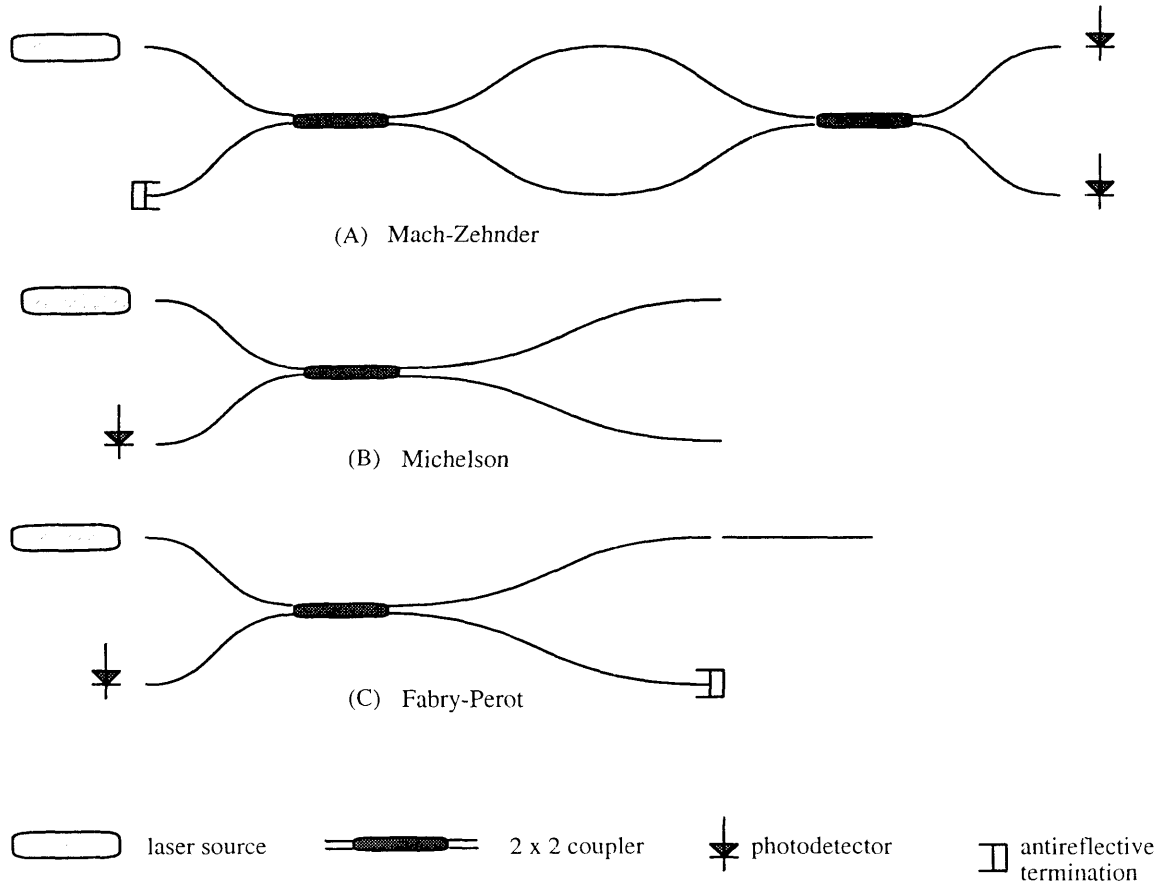

Figure 3.2 Configuration of the three basic optical fibre interferometers.

In the Fabry-Perot interferometer, diagram C in Figure 3.2, the resonant cavity consists of a section of single-mode fibre which is cleaved at both ends to produce optically flat, smooth surfaces. The piece of single-mode fibre is then spliced to one output arm of a fibre coupler so that a very small air gap exists between the face of the coupler fibre and that of the resonant cavity.

An optical fibre interferometer examines variations in the phase difference between two light beams. A phase change is seen as a displacement of the interferometer fringe pattern, with a phase change of 2π causing a displacement of one fringe. A phase change is obtained by causing an alteration in the dimensions and/or refractive index of one arm of the interferometer by subjecting it to a variation in some parameter, such as strain, pressure or temperature and is given by

$$\phi = \frac{2\pi}{\lambda} nL \tag{3.1}$$

where ϕ is the phase, λ is the wavelength of the light, n is the refractive index of the fibre and L is the physical propagation length of the fibre. If the laser source is stable there is no change in the wavelength of the source and differentiating Equation 3.1 gives

$$d\phi = \frac{2\pi}{\lambda} nL\left[\frac{dL}{L} + \frac{dn}{n}\right] \tag{3.2}$$

where $d\phi$ is the change in phase, dL is the change in length and dn is the change in the refractive index of the fibre.

There are advantages and disadvantages in the various interferometric arrangements. The Mach-Zehnder interferometer has two output arms which are $\pi/2$ out of phase. This means that the two outputs can be used to electronically yield a signal which is independent of the source power. Also, the availability of the two outputs means that when small variations in ϕ are to be detected, or measurements are to be taken over long time periods, the sensor can be maintained at the quadrature point, where the interferometer has its maximum sensitivity (Jackson, 1985), by a feedback mechanism. The Michelson interferometer, on the other hand, has only one output, but it is cheaper and simpler to fabricate as only one bidirectional coupler is required and the faces of the interferometer arms can be made simply by cleaving the ends of the fibres. The Michelson interferometer is twice as sensitive as an equivalent Mach-Zehnder interferometer as the light travels twice through the sensing arm of the interferometer. However, both the Mach-Zehnder and the Michelson interferometers have the disadvantage that the reference arm of the interferometer must

be shielded from any parameter which may affect the phase of the light. Furthermore, the entire length of the sensing arm of the interferometer is responsive and so some shielding of the sensing arm may also be required.

The fibre Fabry-Perot interferometer is cheap and straightforward to make, and there is no need for shielding, as the two beams travel along a common path until one beam enters the resonant cavity of the interferometer. As with the Michelson interferometer, the measuring beam traverses the resonant cavity twice.

3.1.2 Optical fibre low-coherence interferometry

All interferometric optical fibre sensors which use a laser as a source suffer from the fact that the output signal varies with a periodicity of 2π radians. Thus, phase changes in one direction are identical to phase changes in the opposite direction and for example, if temperature is the parameter of interest, the total phase change can indicate heating, cooling or a combination of heating and cooling. This need for continual monitoring of the movement of the fringes means that each time a sensor is turned on, the system must be re-set as there is no absolute zero point. A method which allows absolute measurement of quasi-static parameters is optical fibre low-coherence interferometry (OFLCI). A common OFLCI configuration is shown Figure 3.3.

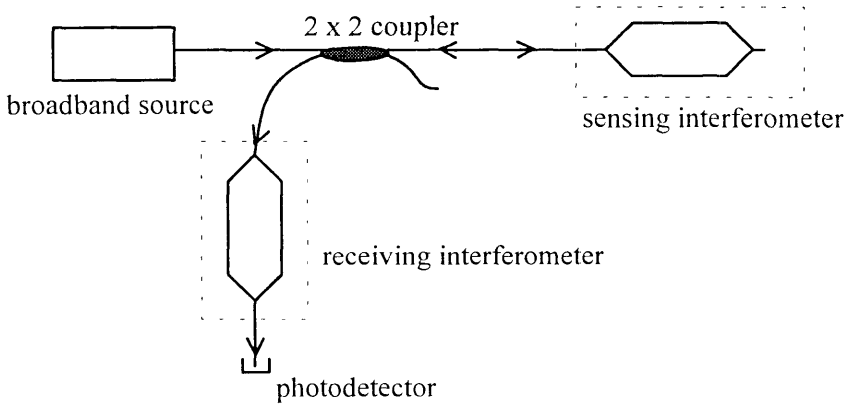

Figure 3.3 Schematic diagram of an optical fibre low-coherence interferometer.

Instead of a coherent light source, such as a laser, a broadband source is used. The output from the sensing interferometer is coupled into a receiving interferometer. The optical path difference (OPD) of the receiving interferometer is adjusted to match that of the sensing interferometer and the output from the receiving interferometer is a function of the difference between the OPDs of the interferometers. Any change in the OPD in the sensing interferometer will result in a change in both the fringe visibility and the phase of the final output signal. The receiving interferometer can track the change in OPD and the change in the central fringe position can be used to determine the absolute OPD change in the sensing interferometer. Rao and Jackson (1996) have published an excellent review article on the progress of this type of interferometry and describe a variety of signal processing techniques. OFLCI requires more sophisticated signal processing and is the best technique to use when absolute measurements are required. However, coherent optical fibre interferometers are ideal when there is no ambiguity in the result.

3.2 *Optical fibre temperature sensors*

Optical fibre interferometers can be made sensitive to a number of parameters, such as electric field (Imai *et al.*, 1986), strain (Butter and Hocker, 1978) and rotation (Jackson, 1985). Optical fibres are intrinsically sensitive to temperature and this has been investigated over many years. When an optical fibre is subject to a change in temperature the light within the fibre undergoes a phase change. When the fibre is in an interferometric configuration the phase change can be measured and Equation 3.2 becomes

$$\frac{d\phi}{dT\,L} = \frac{2\pi}{\lambda}\left[\frac{n}{L}\frac{dL}{dT} + \frac{dn}{dT}\right] \tag{3.3}$$

Using Equation 3.3 and the thermal coefficients of refractive index (dn/dT) and expansion [$(dL/dT) / L$] for pure silica, Hocker (1979) calculated the change in phase per degree per unit length of a silica fibre when the fibre is exposed to a change in temperature. The result was 107 radians/m/deg, equivalent to a fringe displacement of 17 fringes/m/deg. Schuetz *et al.*, (1983) measured the dynamic thermal response of single-mode optical fibres for interferometric sensors and found that the sensitivity is such that a 1 μ°C temperature change can be followed over a frequency range of 50 kHz with a metal-coated optical fibre. Thus, the temperature sensitivity of an optical fibre is such that temperature effects must be carefully considered in any optical fibre interferometric sensor.

Optical fibre temperature sensors are commonly interferometric sensors in both intrinsic and extrinsic configurations. Akhavan Leilabady and Corke (1987) developed an intrinsic temperature sensor using a fibre Fabry-Perot interferometer with a 5 mm resonant cavity on the end of a lead fibre of any desired length. Extrinsic temperature sensors use optical fibres to transmit the light to and from the sensor head and do not use the physical properties of the optical fibre as the temperature sensitive probe. An extrinsic optical fibre interferometer which has been employed by Wolthuis *et al.* (1991) is shown in Figure 3.4. This temperature sensor used the outside surfaces of a thin layer (0.8 μm) of silicon as the resonant cavity. The change in the refractive index of the silicon with temperature is substantial when the wavelength of the interrogating light is close to the bandgap energy of silicon. This sensor was developed for use as a medical temperature sensor. The optical fibre transmits and receives light from the external Fabry-Perot cavity and can be used in areas where electrically active and conducting temperature probes are not appropriate, for example, in the high rf fields associated with hyperthermia treatment for cancer therapy. For high temperature sensing, at temperatures around 1000 °C, Gerges and Jackson (1991) used OFLCI to interrogate a Fabry-Perot interferometer made from a solid fused quartz hemisphere, with a fibre Michelson interferometer as the receiving interferometer.

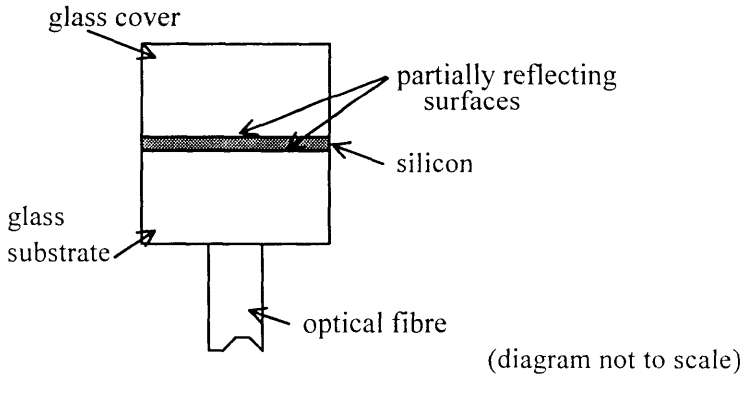

Figure 3.4 Extrinsic temperature sensor using an external Fabry-Perot cavity (Wolthuis *et al.*, 1991).

Each of the temperature sensors described above measures the temperature of a small volume. When the temperature profile across a straight-line path within a heated object is required, an integrated optical fibre temperature sensor can be used. This method assumes that each point in the fibre reaches thermal equilibrium with the surrounding material so that the temperature profile of the fibre replicates the temperature profile of interest. Thus, the total fringe shift measures the integral of the temperature distribution along the fibre. The temperature profile can be recovered by taking a set of measurements at different positions within the region of interest and using deconvolution techniques. Everett *et al.* (1995) used an integrated temperature sensor to measure the temperature distribution within a glow discharge and Scelsi *et al.* (1993) used one to find the temperature distribution within a heated copper plate.

Some optical fibre sensors employ the temperature sensitivity of optical fibres for purposes other than temperature measurement. Hirose *et al.* (1987) have used an optical fibre interferometer as a calorimeter to measure the power of a carbon dioxide (CO_2) laser. Woolsey and Lamb (1992) used an optical fibre interferometer to study the absorption of 10.6 μm CO_2 laser radiation by optical fibres. Both groups exploited the temperature sensitivity of the optical fibre by heating the fibre with a CO_2 laser and recording the phase change.

3.3 *Optical fibre flow sensors*

Optical fibres which are in an interferometer arrangement are very sensitive to vibration and the presence of any intermittent flow around the fibre will cause vibration that is easily detected as a phase change. However, flowmeters generally are required to measure not only the presence of the flow but also the velocity of that flow. Flowmeters have been developed which utilise optical fibres as both extrinsic and intrinsic sensors and exploit the non-electrical nature and the remote sensing capabilities of OF sensors. Optical fibres have also been used to modify existing flowmeters to make them more flexible or easier to handle.

A flowmeter which applies all of the above advantages of OF sensors was developed by Samson *et al.* (1990) for the coal mining industry. In this flowmeter a commercial cup anemometer was modified by mounting reflecting discs on the anemometer spindle. An optical fibre was then mounted so that the frequency of the reflected light was proportional to the spindle rotation rate and hence proportional to the air speed. By using an optical fibre for transmitting the light and receiving

the signal, no underground electrical power was required and many systems could be installed and interrogated through multiplexing techniques. The distance from the sensor to the monitoring point was over 1 km, thus demonstrating the remote sensing capabilities of optical fibre sensors.

Vortex shedder flowmeters use an upstream barrier to create vortices in the flow which are then detected by a sensor downstream. This sensor is conventionally a piezoelectric transducer (PZT) but Chu *et al.* (1990) have replaced the PZT with a Fabry-Perot interferometer made up of either an air cavity or an optical fibre. Both these fibre configurations give performance equal to that of the PZT, the operating temperature range being larger with the optical fibre system.

Conventional laser Doppler anemometry (LDA) has been described in Section 2.6.3 and optical fibres have been employed in LDA to overcome some of the alignment problems associated with the requirement of parallel beams and to make the system more compact. Fibre LDA systems have been developed by Boyle *et al.* (1990) and Stieglmeier and Tropea (1992). An extension of the idea of LDA is an extrinsic optical fibre speed sensor developed by Gogoasa *et al.* (1996). Two optical fibre sensors launch and receive light from a moving surface which has a random reflection profile. If the two sensors are placed a known distance apart there is a time delay between the signals from the sensors and using cross-correlation techniques the time delay between the signals, and hence the speed of the moving surface, can be recovered.

The power generation industry and some chemical industries have a need to measure parameters within flows where both gas and liquid phases are present, one such parameter being velocity. Figure 3.5 shows the details of an optical fibre probe for velocity measurement in these mixed flows (Moujaes, 1990). The probe is based on the fact that the amount of reflection from a chamfered fibre depends on the refractive index mismatch at the fibre-fluid interface. If the fluid is air, or some gas, then there is total internal reflection and light can be coupled into another fibre to be sent back to the detection system. If the fluid has a refractive index larger than that of the fibre some light is coupled out of the fibre and the amplitude of the returning signal is detected. This is shown schematically in diagram A of Figure 3.5. Diagram B shows a schematic diagram of a spherical dual-tipped optical fibre probe for measuring the velocity of gas bubbles within a liquid flow. Two probes are held in close proximity and the gas bubble passing each probe sends back a signal: cross-correlation techniques can then be used to recover the speed of the bubble.

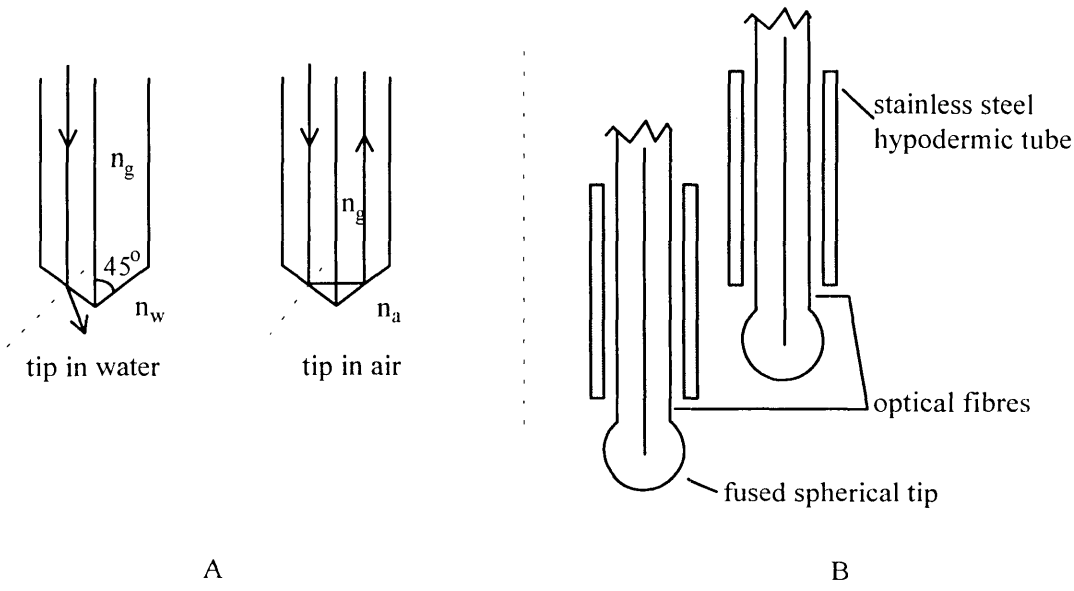

Figure 3.5 Schematic diagrams of optical fibre probes for measuring gas velocity within a liquid flow. A: dual-tipped probe chamfered at 90°, B: spherical dual-tipped probe (Moujaes, 1990).

3.4 The hot-fibre anemometer

Flow-rate sensors which utilise the intrinsic temperature sensitivity of optical fibres are based on the conventional flow measurement technique of hot-wire anemometry, discussed in Section 2.6.2. Samouris *et al.* (1989) developed an optical hot-fibre anemometer to measure the flow rate of nitrogen gas at rates between 0.1 and 2 m/s. This optical hot-fibre anemometer employed a gold-coated optical fibre in one arm of a Mach-Zehnder interferometer. The coated fibre was mounted transversely to the nitrogen flow and heated by a 5-second voltage pulse applied to the gold coating. The nitrogen flow cooled the heated fibre and the overall temperature rise of the fibre, and hence the phase change, was inversely proportional to the nitrogen flow rate.

Lamb and Woolsey (1995) developed an optical fibre technique to measure the speed of the corona wind. They employed a Mach-Zehnder interferometer with the sensing arm held in the discharge gap, normal to the direction of the corona wind. As in the hot-fibre anemometer developed by Samouris *et al.* (1989), the temperature sensitivity of a single-mode optical fibre was exploited by heating a portion of a fibre and exposing this heated portion to a gas flow so that convective cooling

of the fibre took place. The high voltages and electric fields associated with corona discharges ruled out the use of a metal coating for heating the fibre. Hirose *et al.* (1987) have shown that substantial heating of an optical fibre can take place using a pulse from a CO_2 laser and this was the heating method employed for the corona study. Due to the action of the corona wind, the heated section of fibre is cooled by convection and the fringe shift recorded by the interferometer is a function of the speed of the corona wind. The system was calibrated using a known heating regime and a known flow rate of air. Figure 3.6 shows the experimental arrangement used for the corona study. The work of this thesis, using an optical fibre Fabry-Perot sensor (OFFPS), is a development of this earlier work on OF sensing of the corona wind.

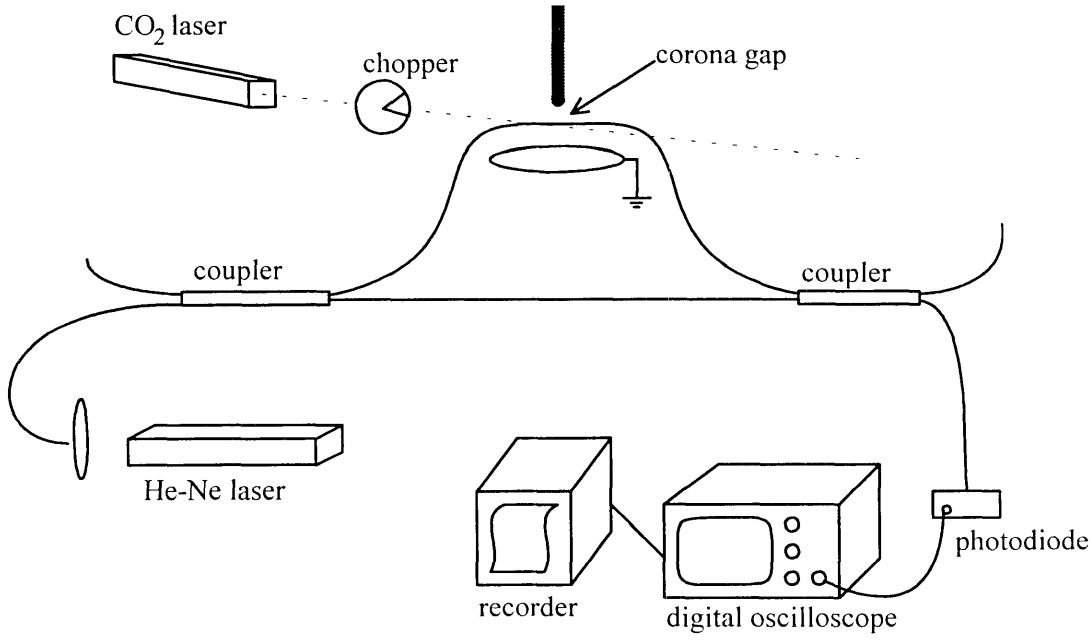

Figure 3.6 Optical fibre interferometer to measure the speed of the corona wind (Lamb and Woolsey, 1995).

Chapter 4

Generation and Measurement of the Corona Wind

In this chapter a description of the discharge system used to generate the corona wind and the systems used to measure the speed of the corona wind will be described. The circuit and electrodes used for all the corona wind measurements are described in Section 4.1. The discharge chamber described in Section 4.2 was used for the optical fibre Fabry-Perot sensor (OFFPS) experiments in both atmospheric air and sulphur hexafluoride (SF_6). The work performed with SF_6 required the addition of a vacuum system and this is described in Section 4.3.

Details of the OFFPS and the computer system used to control the chamber and acquire the data are given in Section 4.4.

The laser Doppler anemometry (LDA) experiment was performed in atmospheric air and used a similar discharge system to that of the OFFPS work, with the exception of the discharge chamber. Section 4.5 details the experimental arrangement for the laser Doppler measurements.

4.1 The discharge system

The discharge circuitry used to produce the corona wind for both the OFFPS and laser Doppler (LD) anemometer measurements is shown in the schematic diagram in Figure 4.1.

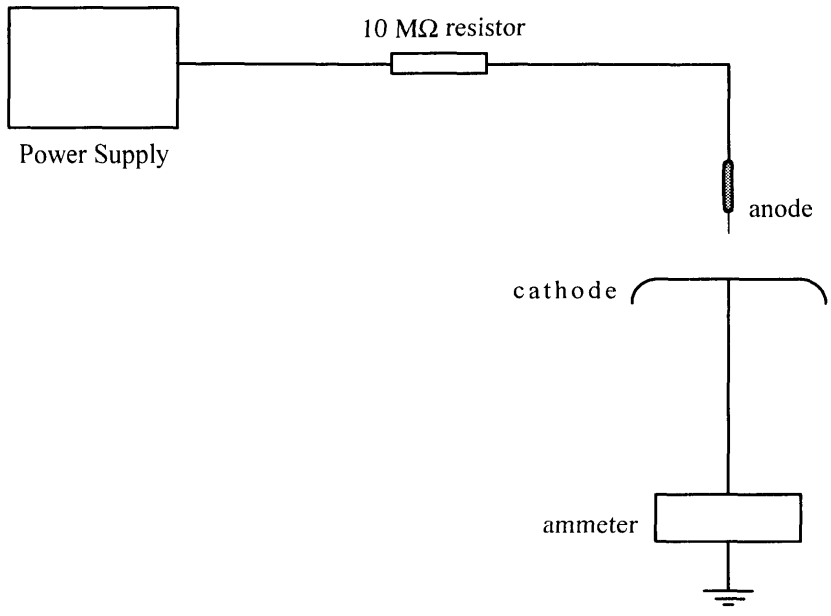

Figure 4.1 Schematic diagram of the discharge circuitry.

The high voltages required to produce the corona discharge were provided by a Hipotronics HV DC Power Supply (0-120 kV). The power supply was connected through a 10 MΩ resistor to the anode of the discharge system. The cathode was connected to ground through a Thurlby 1504 multimeter so that the corona discharge current could be measured. When studying the effect of a current pulse from a corona streamer on the OFFPS, the ammeter was replaced by a LeCroy 9410 Dual-Channel digital oscilloscope and in parallel with a 10 kΩ load resistor. Hard copy from the oscilloscope was obtained by sending digitised traces to a 486-SX IBM-PC computer via a GPIB cable. The applied voltage was measured using the voltmeter associated with the high-voltage power supply and the anode voltage was measured using a high-voltage probe (Tektronix, P6015, 3 pF, 100 MΩ DC, 1000:1 attenuation).

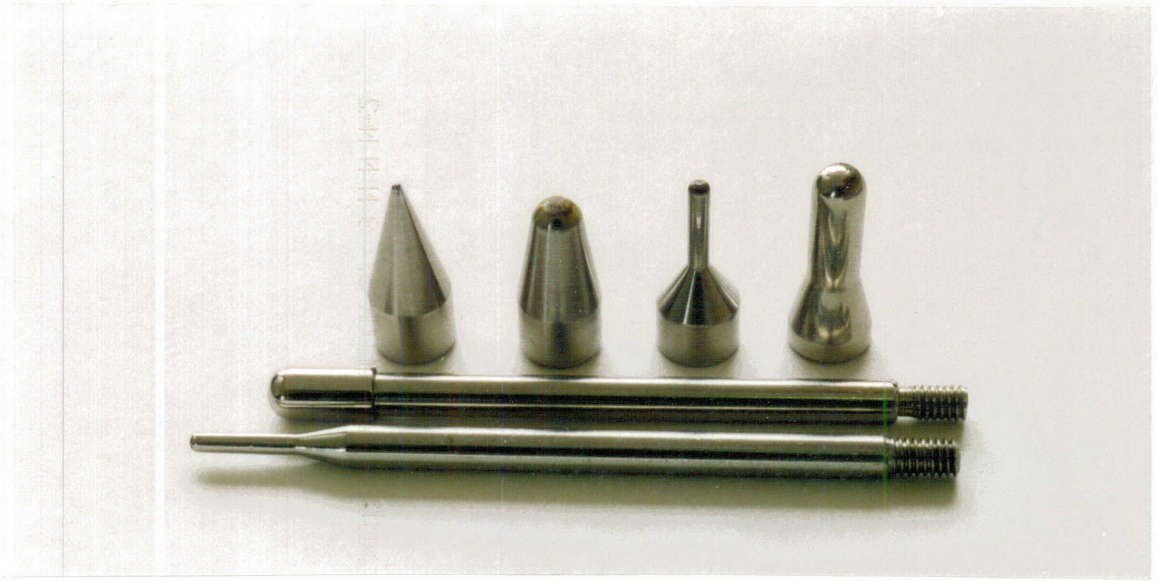

Figure 4.2 Anode tips used to produce the corona discharge

The anode used to generate the corona discharge in the OFS experiments was an 8 mm diameter, 300 mm long stainless steel rod to which any one of four interchangeable stainless steel anode tips could be connected. The anodes were 6° and 15° hyperboloids of revolution and 2 mm and 5 mm diameter hemispherical tips. The two anodes used for the LDA work were 120 mm stainless steel rods with 2 mm and 5 mm diameter hemispherical tips. Pictures of these anode tips are shown in Figure 4.2.

In the OFS system the plane cathode was a disc of stainless steel and in the LDA system the plane cathode was a disc of copper. Both had a diameter of 75 mm and a thickness of 8.5 mm. The edges of the cathodes were machined to a hemispherical profile so that field non-uniformities were minimised. Despite the use of different metals for the cathodes in the two systems, when the other discharge parameters remained constant, the discharge current-voltage characteristics were the same. Refer to Figure 5.6 for an example of the current-voltage characteristics of the OFS dischcarge system.

4.2 The discharge chamber

The discharge chamber used in the OFS experimental work to examine the corona wind in both air and SF_6 (>99.9% purity) is shown in Figure 4.3. The discharge chamber was machined from a single piece of aluminium alloy (type 6351). In each of the six sides of the chamber there was an 80 mm

diameter aperture. These apertures allowed access to the interior of the chamber and could be closed off with an aluminium plate, a window or an electrode mounting. The interior volume of the chamber was 2.9 litres. The chamber was mounted on two parallel 19 mm stainless steel rods via four sets of linear bearings. This mounting allowed horizontal movement of the chamber over a

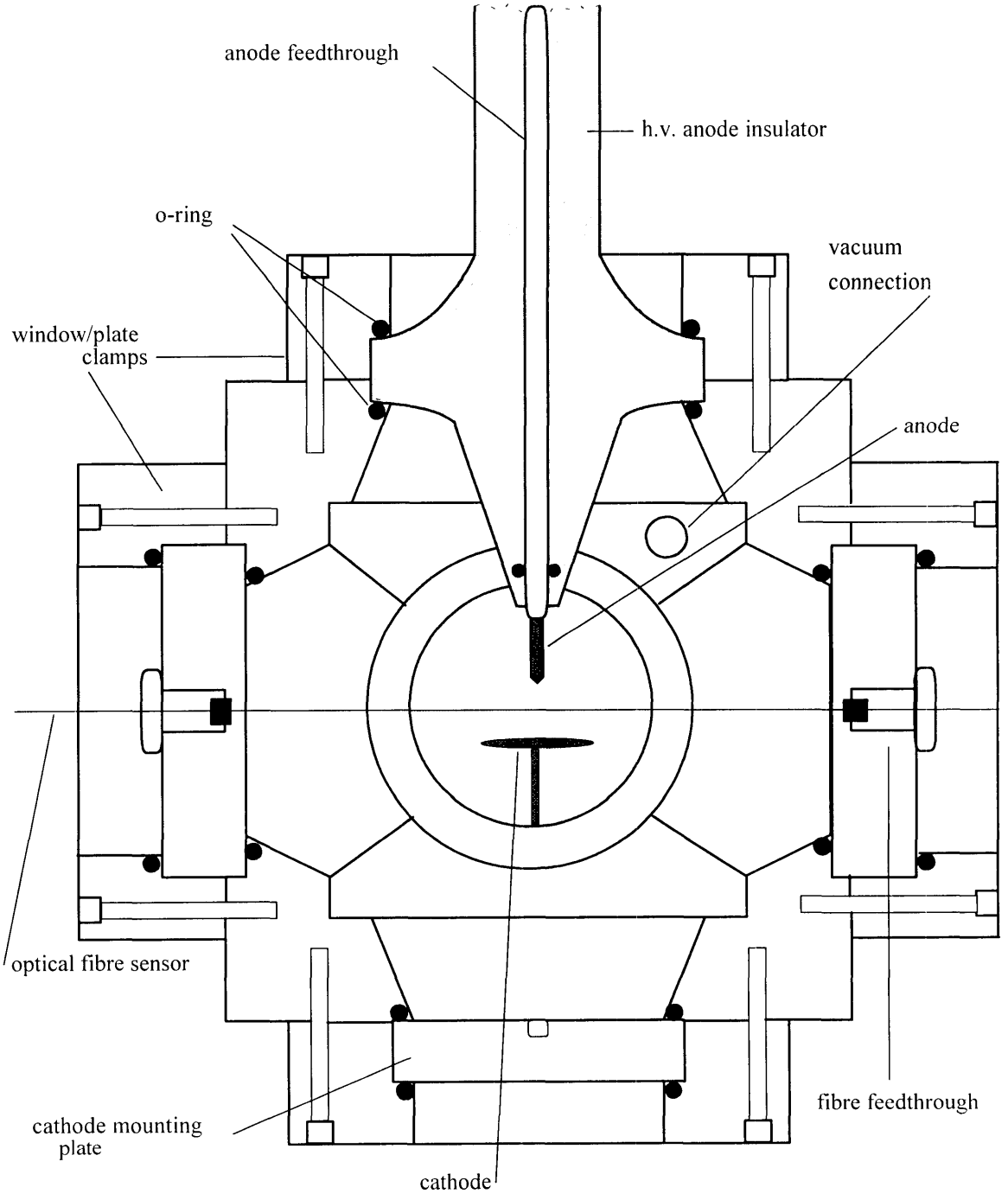

Figure 4.3 Schematic diagram of the discharge chamber.

length of 30 cm. The anode and cathode mounts are shown in Figure 4.4. The cathode was mounted on a stainless steel rod which passed through a nylon base. The nylon base ensured that the cathode was electrically isolated from the discharge chamber, which itself was grounded. The stainless steel rod was connected to a thread which allowed the cathode to be raised and lowered with a precision of 0.2 mm. The cathode was connected to ground through a co-axial cable connector on the exterior of a blank plate which was clamped to the bottom of the discharge chamber.

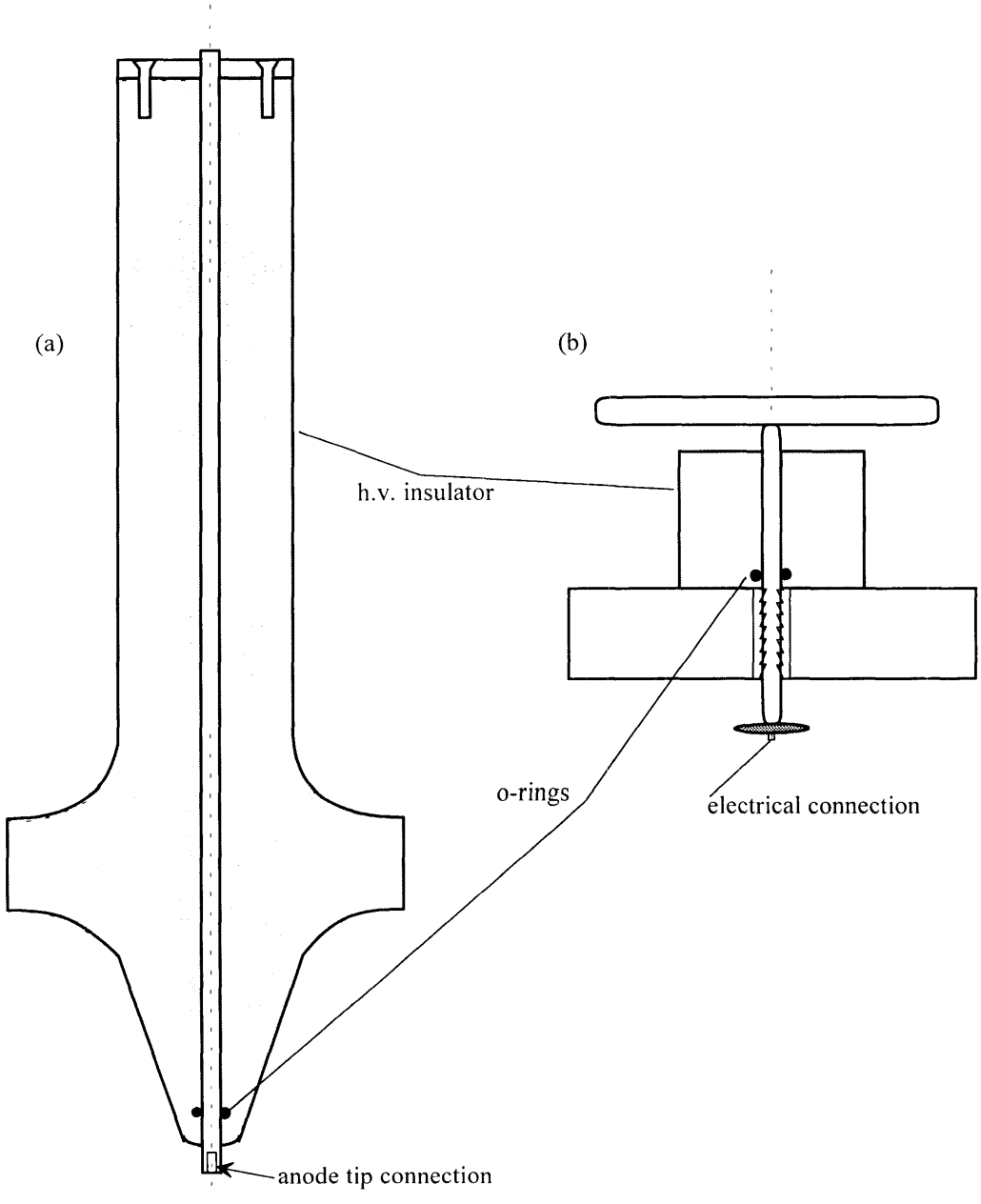

Figure 4.4 Schematic diagrams of (a) anode mount, and (b) cathode mount.

The stainless steel rod was fed, via two 'o' rings, through a nylon rod clamped over the top hole in the discharge chamber. The anode was connected to a threaded rod which allowed the anode to be raised and lowered with a precision of 0.2 mm. Since the fibre was in a fixed position within the chamber, movement of the cathode and anode allowed the position of the fibre within the discharge gap to be varied.

The high voltage cable was connected to the anode feedthrough. The anode feedthrough and the high voltage cable were capped by a 90 mm diameter aluminium dome which prevented external coronas. For safety, a 150 mm diameter plastic tube was placed over the top of the chamber to cover all high-voltage conductors.

The optical fibre entered and exited the chamber through small holes in the centres of blank plates which were attached to opposite sides of the chamber. In order to maintain a vacuum the optical fibre passed through a 5 mm diameter rubber sleeve in each plate and fitted snugly into a screw which had a 0.5 mm hole through its centre, as shown in Figure 4.5.

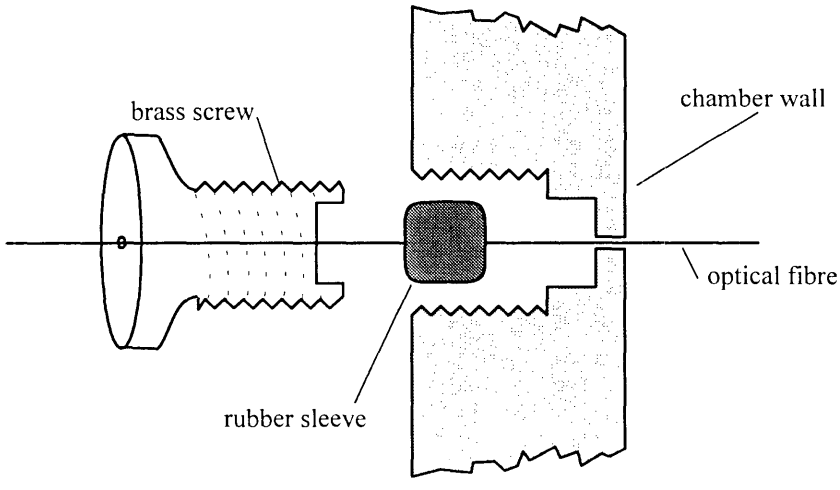

Figure 4.5 An optical fibre feedthrough into the discharge chamber.

When the chamber was used for corona wind measurements in air the remaining two sides of the chamber were left open to atmospheric air. However, for the measurements in the SF_6 discharge, a potassium bromide (KBr) window was sealed onto the end of a 100 mm stainless steel tube which was clamped onto one side of the chamber. The KBr window allowed the CO_2 laser beam access to the chamber. The tube was included so that any decomposition products of the SF_6 discharge would settle out in the tube and thus minimise etching of the window. The side opposite the window was closed off with a stainless steel tube which was designed to prevent reflections from the CO_2 laser re-entering the discharge gap. These two additions are shown in Figure 4.6.

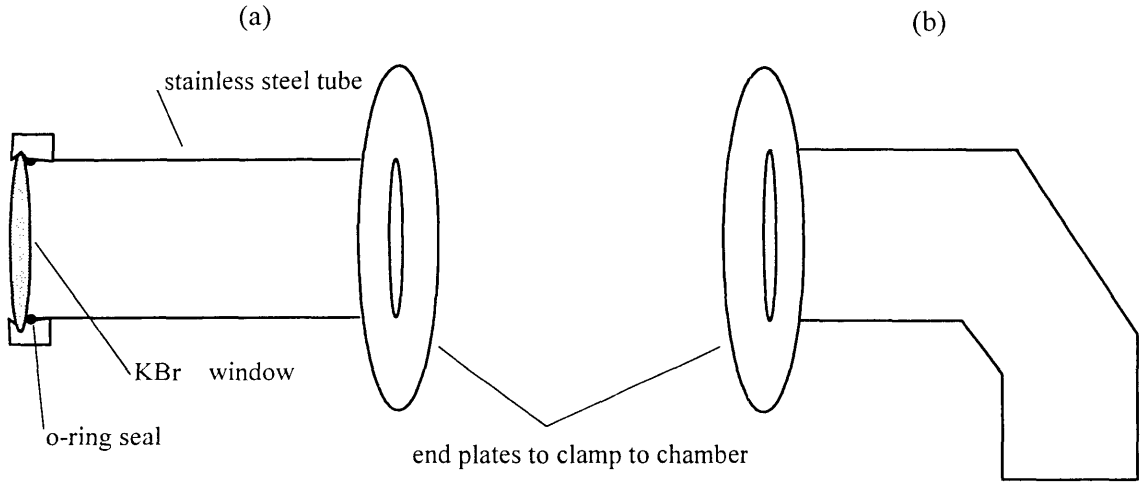

Figure 4.6 (a) CO_2 laser input window, and (b) CO_2 laser beam stop.

4.3 The vacuum system

The vacuum system used for the experimental work in the SF_6 discharge is shown in the schematic diagram of Figure 4.7. The chamber was evacuated to less than 10^{-3} Torr using a Pfeiffer TSU 050 turbo-molecular pump. The base pressure in the chamber was monitored by a Dynavac pressure gauge (10^{-3} - 10 Torr). The SF_6 was introduced into the chamber through an isolation valve and the chamber pressure was monitored by a Penwalt absolute pressure gauge (0 to 210 kPa) connected directly to the chamber. The vacuum system was connected to the discharge chamber using a flange fitting.

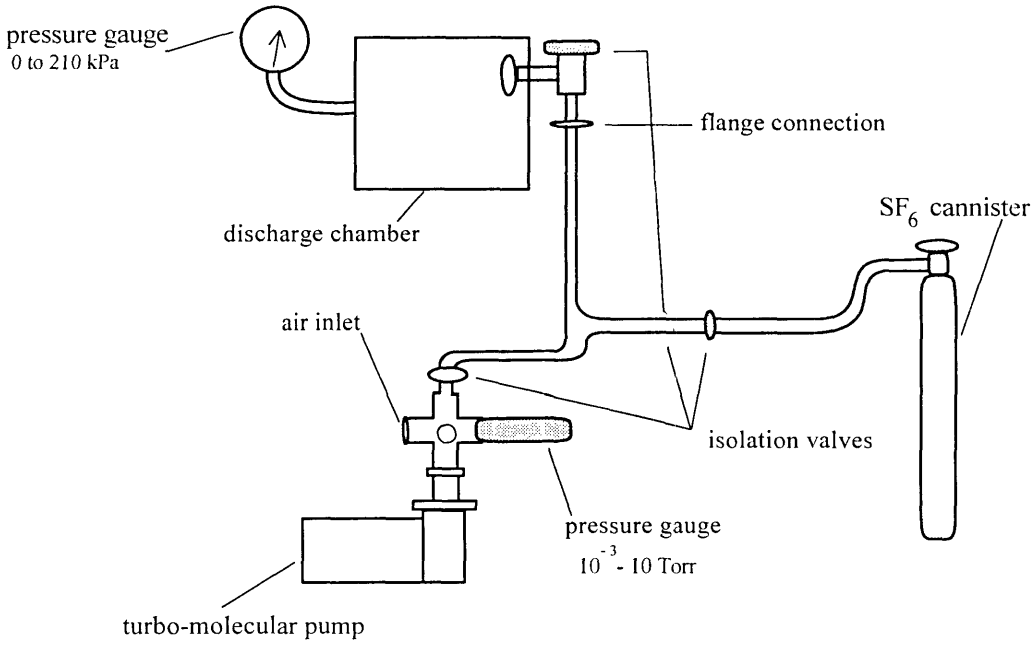

Figure 4.7 The vacuum system used for the SF_6 corona wind measurements.

4.4 The optical fibre Fabry-Perot sensor

A diagram of the entire corona wind speed sensor, data acquisition system and chamber controller is shown in Figure 4.8.

The principle component of the optical fibre sensor is the optical fibre Fabry-Perot interferometer. Light from a 4 mW helium-neon (He-Ne) laser (wavelength - 632.8 nm) was launched into one arm of an ACROTEC 2x2, 633 nm single mode, bi-directional coupler, which provided equal intensities in the two output fibre arms of the coupler. The end of one output arm of the coupler was placed in a small tube of index-matching gel to minimise reflections from that arm. A 150 mm length of fibre, (633 nm, single mode, 4 μm core diameter) was spliced onto the end of the other output arm of the coupler and was used for the Fabry-Perot interferometer. The splice was made using a mechanical splice which had been cleaned of all index-matching gel so there would be sufficient reflection from

the first fibre face for the formation of the Fabry-Perot cavity. Section 3.2 gives further details on optical fibre Fabry-Perot interferometers. This Fabry-Perot cavity made up the sensing element of the OFFPS.

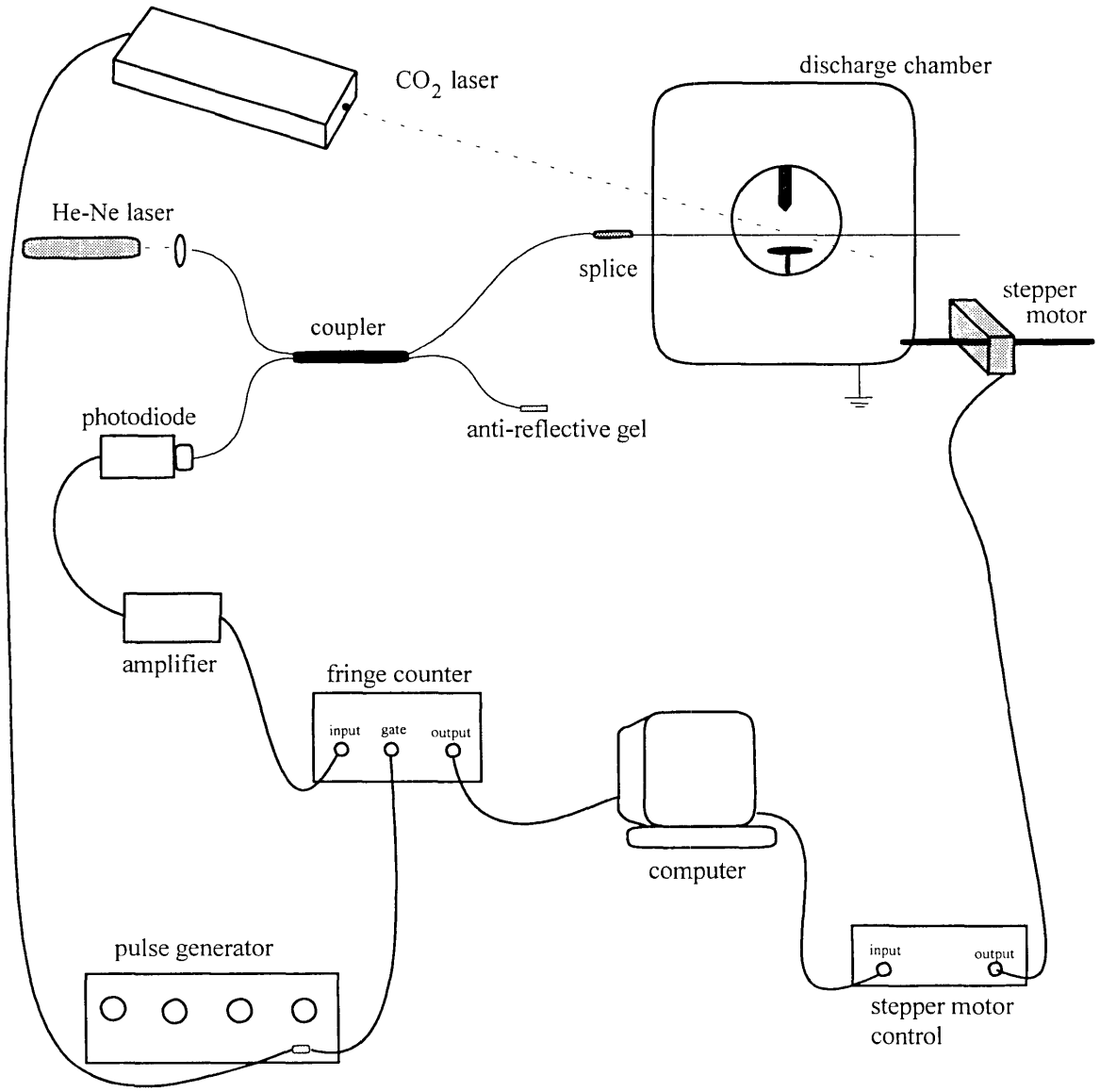

Figure 4.8 The OFFPS arrangement for measurement of the corona wind speed in air and SF_6.

The sensor was introduced into the discharge chamber and held parallel to the plate electrode, and normal to the direction of the corona wind, by the fibre feedthroughs in the discharge chamber (Figure 4.5). Any change in the optical path length of the sensor was seen as interference fringes by a photodiode. A carbon dioxide (CO_2) laser, gated by a pulse generator, was used to heat the sensor in the corona discharge. The maximum temperature reached by the sensor was controlled by the convective effect, and therefore the speed, of the corona wind over the heated portion of the sensor.

For the measurements made in atmospheric air, a 200 ms laser pulse from a 13 W, 10.59 μm wavelength, CO_2 laser (SYNRAD) was used to heat the fibre sensor. The power, at the fibre sensor, from this laser was sufficient to produce interference fringe numbers that gave an experimental uncertainty of less than 1% (more than 150 ± 1 fringes when there was no convective cooling on the fibre sensor). These high fringe numbers allowed the use of two zinc selenide (ZnSe) lenses (focal lengths 38 mm and 80 mm) to focus the CO_2 laser beam to a width of 1 mm at the fibre sensor so that spatial resolution was improved. However, for the measurements taken in SF_6 a laser beam of wavelength 10.59 μm could not be used because SF_6 has a large absorption band at that wavelength (see details in Section 6.1). For the SF_6 measurements a CO_2 grating laser (SYNRAD 48G-2), set at a wavelength of 9.31 μm, was used. The power of the laser at this setting was only 9.0 W in air and absorption of the beam by the KBr entry window and passage through the SF_6 resulted in a decrease in the laser power which reached the fibre. Since the ZnSe lenses would further decrease the power available for heating of the fibre, no beam focussing was used. The beam diameter at the fibre sensor was 4 mm for the measurements taken in SF_6. The grating CO_2 laser required the addition of a refrigerated circulator (Neslab RTE-Series) for laser cooling and in order to maintain a constant power output (± 5%) at the selected wavelength.

The photodiode signal was amplified and fed to a universal counter (Hewlett Packard 5316A) which was gated by the same pulse that gated the CO_2 laser and thus only counted fringes during the CO_2 laser on-time. Counting during the laser on-time enabled environmental influences on the fibre sensor to be minimised. The universal counter was controlled by an IBM-PC via a GPIB cable. The computer acquired the fringe numbers and stored the data to disk.

In order to obtain corona wind speed measurements at off-axis positions across the discharge gap a stepper motor was used to move the entire system of discharge chamber, electrodes and fibre sensor. The stepper motor was an RS stepping linear actuator (318-711) with a step size of 0.025 mm and a lead screw length of 225 mm. With the lead screw of the stepper motor connected to the discharge

chamber, the chamber could be moved over a 170.5 mm length along the two parallel steel rods on which the chamber was mounted. The movement of the discharge chamber with its attached elements meant that the CO_2 laser and its cooling system could remain stationary throughout the experiments. The stepper motor was controlled via the parallel port of the computer. The computer set the universal counter and acquired five sets of data for each chamber position. Then the stepper motor was used to move the discharge chamber so that another set of fringes could be acquired.

4.5 The laser Doppler anemometer

A schematic diagram of the LDA arrangement is shown in Figure 4.9.

The LDA experiment was performed in atmospheric air and did not require the use of the discharge chamber. The electrical system used was that described in Section 4.1 and shown in Figure 4.1. The discharge system and an assembled smoke generator were supported on a two-way translation table which allowed horizontal and vertical movement with 0.2 mm precision (details of the smoke generator are given in Section 4.5.1). The advantage of this arrangement was that it allowed the LD anemometer optical system to remain stationary throughout the experiments.

With a differential LDA system it is very important that the two laser beams which are focussed in the probe volume are initially parallel, have the same polarisation state and have the same intensity (see Section 2.6.3 on the theory of LDA). Once the system is assembled vibrations can cause misalignment of the beams and therefore the entire LDA arrangement was mounted on a Newport table top incorporating pneumatic vibration isolation (Type XL-A). The laser used for the LD anemometer was a 20 mW He-Ne laser (Spectra Physics) with a wavelength of 632.8 nm. The laser beam was incident on an Oriel beamsplitter device. The beamsplitter consisted of two 90° triangular prisms glued together and a single right-angle triangular prism, mounted 60 mm apart. To enable the two emerging beams to be parallel to within 1 minute of an arc, the cube and prism were each mounted on a Newport tilt/rotation stage which allowed two independent tilt directions and an in-plane rotation adjustment. The beamsplitter device and mounts are shown in Figure 4.10.

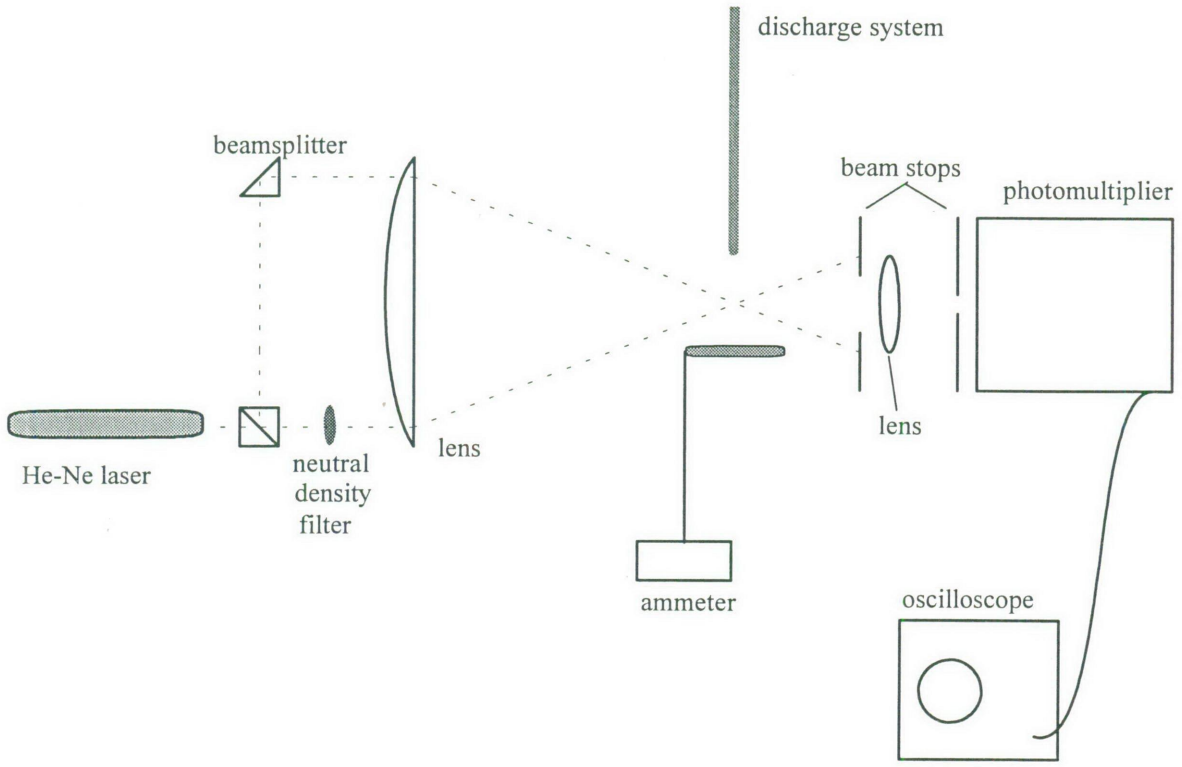

Figure 4.9 The laser Doppler anemometry arrangement for measurement of the corona wind speed in air.

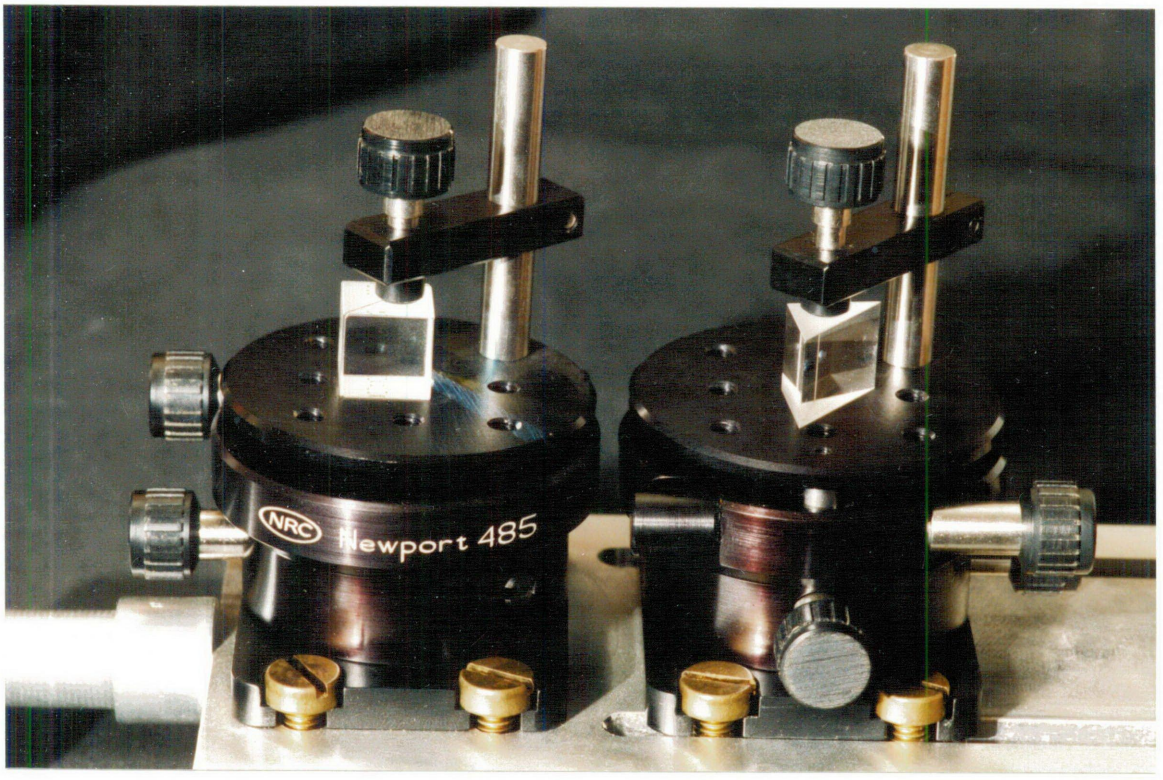

Figure 4.10 The beamsplitter mounts used to ensure parallelism of the emerging beams.

The required degree of parallelism was achieved by placing a glass window (100 mm in diameter, 27 mm thick) on the optical bench in front of the beamsplitter so that the reflected beams, after projection over 15 m, could be accurately aligned. The back side of the window was frosted so that there was no problem with double reflections.

For maximum fringe visibility the two beams needed to be in the same polarisation state. Due to the nature of the reflections within the beamsplitter the emerging beams only had the same polarisation if the plane of polarisation of the incident beam was either parallel or perpendicular to the incident face of the beamsplitter. To achieve this the two emerging beams were first directed through a linear polariser and the laser rotated until the beams were in the same polarisation state.

The Oriel beamsplitter had an Inconel 30:30 coating at 45° incidence which gave 38% transmission and 19 % reflection when the laser was aligned parallel to the incident face of the beamsplitter. A 50% neutral density filter was used to reduce the intensity of the transmitted beam to that of the reflected beam.

The beams were focussed to the probe volume by a lens of 80 mm diameter and 250 mm focal length. The primary diverging beams were stopped using a variable aperture which allowed the scattered light from the probe volume to be gathered by a lens of 50 mm focal length and focussed onto a 2 mm aperture in front of the photomultiplier. The photomultiplier was an EMI 9658 tube which was housed in a cooling chamber (Products for Research Inc., TE-149). The chamber allowed the photomultiplier to be cooled to a temperature of -50°C. The signal from the photomultiplier was fed to the LeCroy 9410 Dual-Channel digital oscilloscope which was used in single-shot mode to capture the occasional Doppler signal from a seeding particle. The oscilloscope had a fast Fourier transform (FFT) option and this was used to determine the frequency of the Doppler signal. To determine the wind speed at any one position the frequencies from five to ten Doppler signals were averaged.

4.5.1 The smoke generator

In order to obtain clear Doppler signals, particle seeding of the corona discharge was required. A smoke generator was used which introduced the seeding particles into the discharge gap from above

the anode tip. The pressure reduction around the anode, caused by the presence of the corona wind, draws the particles into the gap.

The seeding particles were produced by dripping a liquid, known as Rosco Fog Fluid, onto a heater element, as indicated in Figure 4.11. The fluid evaporated and a dense fog was produced. The fog fluid (manufactured by Rosco Laboratories Inc.) consists mainly of an ox bile extract and is made up of salts of glycoholic and taurochloric acids ($C_{26}H_{43}NO_6$ and $C_{26}H_{45}NO_7S$, respectively) (Woerner, 1988).

The fog fluid was held in a reservoir attached to a gravity-fed drip-feedthrough. The drip-feedthrough was held above the heater element. A heater voltage of 18 V was required to evaporate the fog fluid dripping onto the element.

A 200 mm-side cubic perspex box, with an outlet directly above the discharge gap, contained the fog particles. The entire arrangement of Figure 4.11 was connected to a two-way translation table. The plate electrode was mounted on the perspex base and the anode cable was fed through the box with the anode emerging through the outlet in the base of the box. The fog condensed on all surfaces with which it made contact and, in order to minimise the amount of condensation on the electrodes, a plastic plug was designed to neatly fit the end of the anode cable, as shown in the inset diagram in Figure 4.11. Fog fluid which condensed on the cable ran down and gathered in a trough in the insert and then ran out the 'fluid outlet' holes onto the floor of the perspex box. The fog was drawn into the insert through 'fog inlet' holes by the pressure drop at the anode tip and flowed into the corona discharge gap. Although some of the fog particles, which seeded the corona wind, did condense on the anode and cathode, the levels of condensation were small and periodic wiping of the electrodes allowed a stable corona discharge to be maintained.

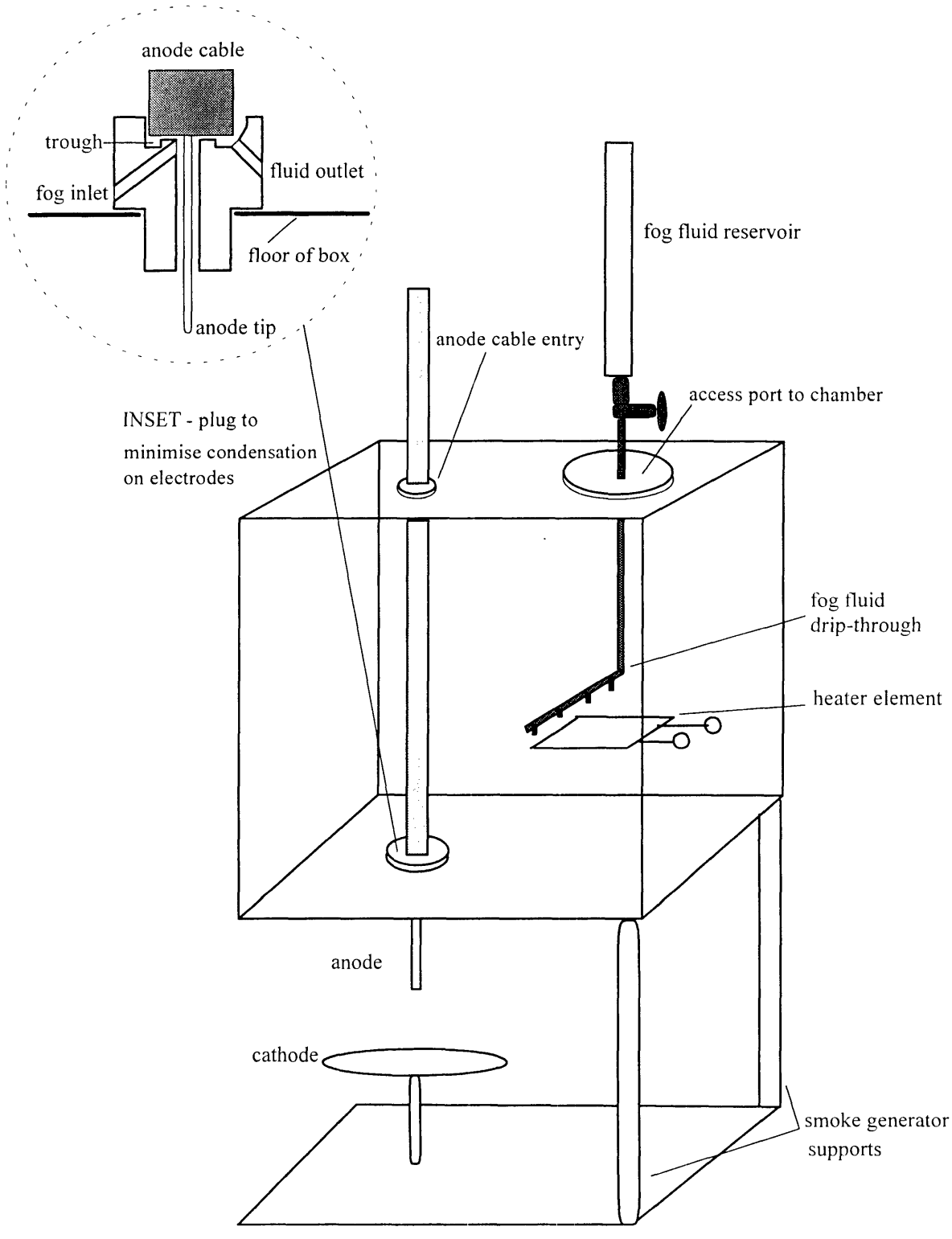

Figure 4.11 The smoke generator and discharge support with details of the plug to minimise condensation of fog fluid on electrodes.